


Article

Synthesis and Properties of a Photocurable Coating Based on Waste Cooking Oil

Mengyu Liu, Yan Liu, Pengyu Wang, Wanying Ying, Qing Liu, Guanzhi Ding and Shuoping Chen * 

College of Materials Science and Engineering, Guilin University of Technology, Guilin 541004, China; 2120210291@glut.edu.cn (M.L.); 2120200279@glut.edu.cn (Y.L.); 2120220368@glut.edu.cn (P.W.); 2120210327@glut.edu.cn (W.Y.); 2120220336@glut.edu.cn (Q.L.); 1020220195@glut.edu.cn (G.D.)

* Correspondence: 2012014@glut.edu.cn

Abstract: In order to provide a cost-effective solution for photocurable coatings and introduce a novel approach for utilizing waste cooking oil (WCO), a type of photocurable resin based on WCO was synthesized. This WCO-based coating incorporated epoxy waste oil methacrylate (EWOMA) derived from WCO and 2-hydroxyethyl methacrylate (HEMA) as a second monomer. It allowed for easy application and rapid curing when exposed to 405 nm purple light. The cured coating, with an optimized composition of EWOMA: HEMA = 4:1 in mass ratio, exhibited favorable mechanical properties (tensile strength: 9.3 MPa, elongation at break: 38.1%) and demonstrated good coating film performance. The coating film exhibited good adhesion (grade 2), high pencil hardness (2H), excellent impact strength (62 kg·cm⁻¹) and low aldehyde content (0.34 μg·g⁻¹). Moreover, it showcased excellent antimudge properties, with a low percentage of water-based ink residual (6.8%), which could be effortlessly and completely removed by wiping. Additionally, the WCO-based coating demonstrated impressive anticorrosive properties, as evidenced by the intact coating film on the tinplate that remained corrosion-free for over 20 days in brine. This cost-effective WCO-based coating offers a viable alternative to commercial photocurable coatings.

Keywords: photocurable coating; waste cooking oil; 2-hydroxyethyl methacrylate



Citation: Liu, M.; Liu, Y.; Wang, P.; Ying, W.; Liu, Q.; Ding, G.; Chen, S. Synthesis and Properties of a Photocurable Coating Based on Waste Cooking Oil. *Coatings* **2023**, *13*, 1553. <https://doi.org/10.3390/coatings13091553>

Academic Editor: Je Moon Yun

Received: 8 August 2023

Revised: 31 August 2023

Accepted: 4 September 2023

Published: 5 September 2023



Copyright: © 2023 by the authors. Licensee MDPI, Basel, Switzerland. This article is an open access article distributed under the terms and conditions of the Creative Commons Attribution (CC BY) license (<https://creativecommons.org/licenses/by/4.0/>).

1. Introduction

As an inedible catering waste, waste cooking oil (WCO) can pose serious public health hazards and contribute to environmental pollution [1–5]. However, with the right processing strategy, WCO can be a valuable renewable resource. Current mainstream technologies for reutilizing WCO involve transforming it into various products, such as biodiesel [6,7], bio-lubricants [8–10], biosurfactants [11], alkyd resin [12–14], and cleaning products [15], among others. Due to high market demand, biodiesel production from WCO has become the primary method of utilizing WCO. When compared to biodiesel derived from natural oil sources, such as palm oil, soybean oil, peanut oil, and olive oil, WCO-based biodiesel stands out for its superior cost-effectiveness, characterized by reduced energy consumption and a diminished carbon footprint in the form of lower greenhouse gas emissions. However, due to its relatively low-profit margin, large-scale biodiesel production requires a sustainable and abundant supply of resources, which is heavily influenced by the prices of WCO feedstock. Moreover, biodiesel production necessitates high-quality WCO feedstock with low levels of free fatty acids and appropriate fatty acid compositions. It also involves laborious pre-treatment steps for WCO, such as decolorization, deodorization, degumming, filtration, clarification, or dehydration, as well as the use of catalysts with relatively high preparation costs [16–21]. Overall, large-scale biodiesel production from WCO is suitable for economically robust areas but may not be the best choice in regions where oil sources and the economy are scarce. In our recent report, we achieved the conversion of WCO into functional materials on a smaller industrial

scale but with higher technology and added value. These materials include 4D printable photocurable resin [22], wax [23,24], or solid alcohol [25]. Such approaches may represent better strategies for WCO utilization in economically underdeveloped areas.

The UV photocurable coating possesses numerous remarkable advantages, including high curing efficiency, high coating hardness, low curing energy consumption, low volatility, and environmentally friendliness [26–31]. It has found widespread application in industries such as wood coating [32], plastic coating [33], decorative building materials [34], electronics [35], and more. Presently, the predominant photocurable coatings mainly employ petroleum-based acrylates [36,37], acrylamides [38], or ethylene glycols [39] as prepolymers. However, with the growing emphasis on sustainable development and ecological economics, stricter regulations have been imposed regarding the use of petroleum-based raw materials. The growing urgency to explore renewable polymeric materials derived from biomass, such as cellulose [40,41], lignin [42,43], and plant oil [44,45], has become increasingly evident. Among these biomass sources, plant oils have gained significant recognition for their pivotal role in producing functional and sustainable polymeric materials and additives. These versatile materials encompass plasticizers [46,47], coatings [48,49], thermosetting resins [50,51], composite materials [52,53], and even 3D printing materials [54]. The key to unlocking the potential of plant oils lies in the profound functionalization and modification of the triglycerides they contain. This process yields valuable derivatives, including unsaturated esters [55,56], epoxides [57], and ethylene oxides [58,59], which can be harnessed as polymer monomers. Epoxidation, in particular, emerges as a preeminent method for modifying plant oils due to its favorable attributes: mild and controllable reaction conditions, straightforward execution, cost-effectiveness, and applicability across a broad spectrum of oil sources [60]. Epoxidized plant oils can be further utilized in the creation of thermosetting materials through their reaction with specific carboxylic acid monomers [52,61]. This innovative approach opens the door to the design of novel functional polymers with attributes like renewability, recyclability, or repairability [62–64]. Taking this a step further, molecular modifications of epoxidized plant oils, such as the grafting of unsaturated carboxylic acid ester moieties onto the epoxy groups, yield monomers endowed with photopolymerization capabilities [65,66]. This advancement paves the way for the development of environmentally friendly biomass-based UV-curable coatings. Notably, one of the most frequently cited monomers in this context is epoxidized soybean oil acrylate (ESOA), which demonstrates the ability to undergo photopolymerization upon exposure to UV radiation in the presence of a suitable photoinitiator. ESOA can serve as a standalone monomer for the formulation of photocurable coatings or be combined with other monomers like hydroxyethyl methacrylate to create high-performance photocurable coatings [67–71].

In contrast to resins based on soybean oil (SO), polymers manufactured from waste cooking oil (WCO) as their primary source exhibit remarkable benefits. These advantages encompass reduced expenses, heightened sustainability, and an improved ecological footprint. Moreover, they do not encroach upon resources required for food production [72]. Though pure acrylate WCO molecules can also undergo photopolymerization with an appropriate photoinitiator under UV radiation, there are still significant hurdles to overcome before it can be considered a practical coating. Firstly, WCO is known to contain a variety of impurities characterized by its dark color and unpleasant rancid odor. These impurities can significantly compromise the quality of the final product unless appropriate pretreatment measures are undertaken. Secondly, the high molecular weight of liquid acrylic WCO contributes to its elevated viscosity, posing challenges during the coating process and increasing the likelihood of defects in the finished coating. Thirdly, the WCO molecule's highly flexible configuration and the relatively low density of unsaturated double bonds result in the cured product of pure acrylic WCO exhibiting weak mechanical properties. Consequently, this leads to poor coating performance, including low hardness, adhesion, and impact strength.

In our recent work, we proposed a new strategy for preparing a practical photocurable resin based on WCO, which involved two key steps [22]. To begin, we employed the “epoxidation & ring-opening esterification” method as a primary step in the production of acrylate-based WCO. Epoxidation was proven to be a highly effective approach for WCO modification, and it could be conducted under mild reaction conditions (below 70 °C and at atmospheric pressure). The epoxidation reagent, containing peracetic acid, was synthesized through the reaction of hydrogen peroxide and glacial acetic acid. The surplus peracetic acid, serving as a potent oxidant, facilitated the peroxidative degradation of various colored and odorous organic impurities within the WCO, thus eliminating the rancid odor and enhancing its coloration. Furthermore, this epoxidation process also targeted the unsaturated double bonds in the WCO, transforming them into epoxy groups that formed the foundation for subsequent ring-opening esterification. Consequently, we obtained epoxy waste cooking oil (E-WCO) as an intermediate product, which could then undergo further reactions with methacrylic acid or acrylic acid to yield practical photocurable monomers within the acrylate WCO category. Subsequently, we introduced appropriate secondary monomers to blend with the acrylate WCO, creating a practical photocurable resin. These secondary monomers played a dual role, functioning as active diluents to reduce the viscosity of the liquid resin while simultaneously forming polymeric segments within the curing resin. These polymeric segments often exhibited superior mechanical properties compared to the WCO segment, effectively absorbing energy and enhancing the resin’s resistance to external stress. This construction resulted in a network that enhanced the mechanical properties and other characteristics of the WCO segment. Using this strategy, we synthesized a WCO-based resin containing epoxy waste oil methacrylate (EWOMA), which was synthesized using the “epoxidation & ring-opening esterification” method on WCO. We also introduced 2-phenoxyethyl acrylate (PHEA) and methacrylic acid (MAA) as additional monomers. The WCO-based resin demonstrated high flexibility, functional pressure-sensitive adhesion properties, and good thermally induced shape memory performance. It had the potential to be used as a multifunctional polymer consumable for 4D printing.

In order to develop a practical photocurable coating, we synthesized EWOMA using the “epoxidation & ring-opening esterification” method on WCO based on our previous work [22]. Furthermore, in consideration of the requisite hardness and adhesion criteria for coatings, we introduced 2-hydroxyethyl methacrylate (HEMA) as a supplementary monomer to blend with EWOMA. This innovative combination marked the inaugural development of a practical photocurable coating utilizing WCO as its primary raw material, as illustrated in Figure 1. This WCO-based photocurable coating boasted a multitude of remarkable attributes, including cost-effectiveness, exceptional adhesion, elevated hardness, commendable impact resistance, resistance to ink, and anti-corrosive properties. In this work, we conducted comprehensive testing, analysis, and reporting on the mechanical and coating properties of the resultant WCO-based photocurable coating. Furthermore, we delve into an in-depth exploration of the influence exerted by EWOMA and HEMA on the properties of the WCO-based resin.

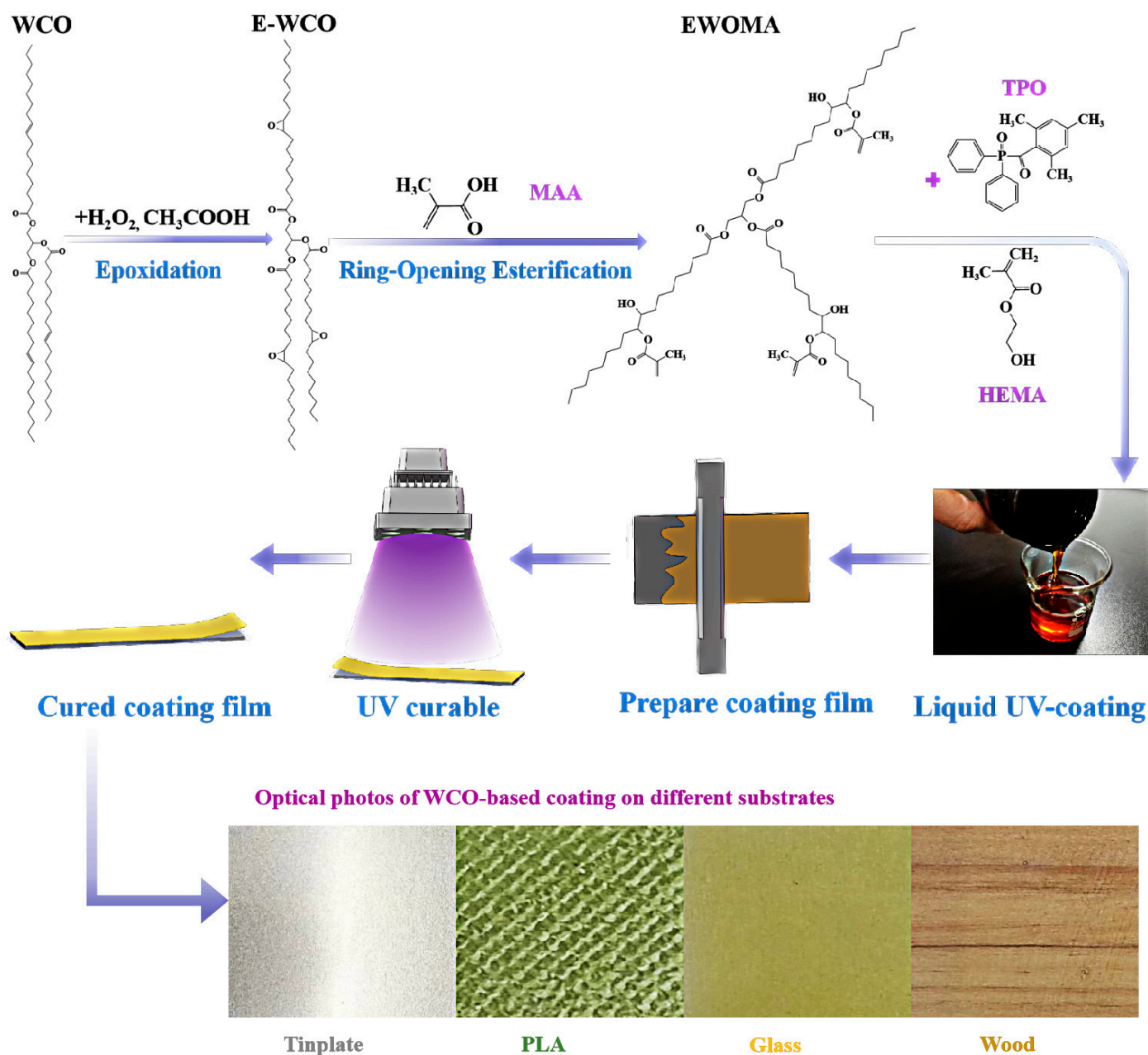


Figure 1. Schematic illustration of the synthesis, application and curing of the photocurable coating based on WCO.

2. Materials and Methods

2.1. Materials

The waste cooking oil (WCO, iodine value: 83.0) was collected from the three-phase separator of Guilin Bioland Renewable Energy Co., Ltd. Sulfuric acid (98%) and hydrogen peroxide (H_2O_2 , 30 wt% in H_2O) were sourced from Xiya Chemical Technology Co., Ltd. in Linyi, China. Urea (99% purity), acetic acid (99.5% purity), sodium bicarbonate (NaHCO_3 , 99.5% purity), methacrylic acid (MAA, 98% purity, stabilized with 250 ppm 4-methoxyphenol), triphenylphosphine (PPh_3 , 99% purity), hydroquinone (HQ, 99% purity), 2-hydroxyethyl methacrylate (HEMA, 96% purity, containing 250 ppm MEHQ stabilizer), and diphenyl (2,4,6-trimethylbenzoyl) phosphine oxide (TPO, 97% purity) were all procured from McLean Company in Shanghai, China. All synthetic reagents, except for the WCO feedstock, were used without further purification.

2.2. Synthesis of the WCO-Based Photocurable Coating

In this study, the WCO employed had a characteristic dark brown appearance accompanied by an unpleasant rancid odor, characterized by a relatively high iodine value of 83.0. Analysis conducted through GC-MS (see Table S1 in ESI) revealed that oleic acid constituted the highest proportion among the triglycerides present in the WCO, accounting for a mass fraction of 68.3 wt%. This indicates that the raw oil contained a significant amount of unsaturated double bonds, which is beneficial for enhancing mechanical properties.

Using the collected WCO as a raw material, epoxy waste oil methacrylate (EWOMA) was synthesized following our previous work [22]. Firstly, a mixture of 620 g 30% H₂O₂, 160 g glacial acetic acid, 4 g concentrated sulfuric acid, and 4 g urea was prepared in a lightproof container and placed in an oven at 40 °C for 12 h to obtain peracetic acid as the epoxidation reagent. Next, 1000 g of WCO was placed in a glass-stirred reactor and heated to 40 °C, and the prepared epoxidation reagent was slowly added to the reactor over a period of 2 h. The reaction mixture was subsequently heated to 70 °C and maintained at this temperature for a duration of 3 h. Following the completion of the reaction, the mixture underwent a 12-h period of standing to facilitate stratification. The upper oil layer was then collected, subjected to a single wash using a 5% NaHCO₃ solution, and subsequently washed twice with deionized water at a temperature of 60 °C. The mixture was further subjected to vacuum evaporation at 70 °C. Upon cooling, the resulting product was identified as epoxy waste cooking oil (E-WCO), appearing as a light yellow liquid devoid of any odor and possessing an epoxy value of 4.37. During the epoxidation process, a significant reduction in the rancid odor of the WCO was achieved, and its color underwent notable improvement. The initial dark brown supernatant liquid of WCO exhibited a high Lovibond color value (Y = 50.5 and R = 20). However, post-epoxidation, the resulting epoxy waste cooking oil (E-WCO) exhibited a considerably lighter color, shifting towards yellow and presenting a reduced Lovibond color value of Y = 10 and R = 1 (refer to Table S2 in the ESI for details). Next, in a three-neck flask, 100 g of the acquired E-WCO was combined with 0.1 g of HQ while being stirred at 90 °C, resulting in the formation of a homogeneous solution. Simultaneously, in a separate container, a mixture of 34.1 g of MAA and 1 g of PPh₃ was prepared at 60 °C to create another homogeneous solution. The MAA solution was then slowly introduced dropwise into the E-WCO solution using a constant pressure dropping funnel. The ensuing reaction mixture was heated and stirred at 100 °C for a duration of 4 h, ultimately yielding EWOMA in the form of a yellow, transparent liquid.

Subsequently, the obtained EWOMA monomer was blended with HEMA in various mass ratios at 60 °C, as specified in Table 1. The initiator (TPO) was introduced at a dosage of 3 wt% relative to the combined monomers, and the mixture underwent stirring at 60 °C until the formation of a clear, yellow solution. Upon cooling to room temperature, a range of photocurable resins based on WCO was obtained, presenting as clear yellow liquids. These resins could be directly utilized as photocurable coatings and efficiently cured under 405 nm purple light.

Table 1. The synthetic formula of WCO-based coatings.

Sample	EWOMA Dosage (g)	HEMA Dosage (g)	Mass Ratio of EWOMA to HEMA	TPO (g)
A1	100	50	2:1	3
A2	150	50	3:1	4
A3	200	50	4:1	5
A4	250	50	5:1	6
A5	300	50	6:1	7
EWOMA (control sample)	100	-	-	2

2.3. Application and Curing of the WCO-Based Photocurable Coating

The roll-coating of the WCO-based coating was performed on a tinplate measuring 120 × 50 × 0.5 mm using an SZQ coating applicator (Kexin, Tianjin, China), following the China Standard GB/T 1727-1992 [73]. The curing process was carried out using a

20 W 405 nm purple light lamp with an illuminance of 8×10^4 LUX. The curing UV light source employed emits primarily at a maximum wavelength of 405 nm, with emissions spanning between 340 and 455 nm. As illustrated in Figure S1 within the ESI, there was a notable alignment between the emission spectrum of the light sources and the absorption spectrum of the liquid WCO-based resin. Consequently, the resultant WCO-based photocurable coating could be efficiently cured utilizing a 405 nm purple light lamp.

After irradiation under the 405 nm purple light lamp for 10 min, a pale yellow cured WCO-based coating with a thickness of $150 \pm 8 \mu\text{m}$ was obtained and could be directly used for various coating property tests. Similar procedures can be applied to achieve roll-coating on glass, plastic, and wood surfaces (see Figure 1).

2.4. Characterization

The iodine value of the oil and the epoxy value of E-WCO were assessed in accordance with the China Standards GB/T 5532-2008 [74] and GB/T 1677-2008 [75], respectively. To determine the composition of various fatty acids in WCO, the method specified in China Standard GB 5009.168-2016 [76] was followed, which involved the preparation of methyl esters analyzed using a 7890-5979 gas chromatography-mass spectrometer from Agilent, Santa Clara, USA. The aldehyde content of the samples was determined in line with GB/T 14571.3-2008 [77]. The color codes were evaluated using a LABO-HUB WSL-2 Lovibond tintometer (Xinrui, Shanghai, China). The UV-VIS absorption spectrum was acquired via a UV3100 UV-VIS-NIR spectrophotometer originating from Shimadzu, Tokyo, Japan.

The photo-differential scanning calorimetry (P-DSC) experiments on the liquid coating were carried out using a DSC 6000 differential thermal analyzer (PerkinElmer, Waltham, MA, USA) with a 30 mW, 405 nm visible irradiation source. The infrared (IR) spectra of the uncured and cured coating were recorded as KBr pellets in the range of $400\text{--}4000 \text{ cm}^{-1}$ on a Nicolet 6700 FT-IR spectrometer (ThermoFisher, Waltham, MA, USA) with a spectral resolution of 4 cm^{-1} . X-ray photoelectron spectroscopy (XPS) analysis of the cured coating was conducted using an ESCALAB 250Xi X-ray photoelectron spectrometer originating from ThermoFisher, Waltham, MA, USA, employing Al $K\alpha$ X-ray radiation for excitation.

Thermogravimetric analysis was conducted using a TG 209 F1 Libra thermal gravimetric analyzer (Netzsch, Selb, Germany) at a heating rate of $10 \text{ }^\circ\text{C}/\text{min}$ within the temperature range of $30\text{--}650 \text{ }^\circ\text{C}$ under a nitrogen gas atmosphere. Differential scanning calorimetry (DSC) tests were carried out utilizing a DSC 204/2920 differential scanning calorimeter originating from TA Instruments, New Castle, DE, USA. The value of the glass transition temperature (T_g) was read from the DSC curve. Dynamic thermomechanical analysis (DMA) was performed using a DMA861e dynamic thermomechanical analyzer (Mettler Toledo, Zurich, Switzerland) operating in the stretch mode under an air atmosphere, spanning the temperature range of -80 to $150 \text{ }^\circ\text{C}$. The heating rate employed was $3 \text{ }^\circ\text{C}/\text{min}$, with a frequency of 1 Hz. Test samples were 3D printed in the form of rectangular strips (size: $25 \text{ mm} \times 5 \text{ mm} \times 0.6 \text{ mm}$). The crosslinking density (v_e , mol/cm^3) of the sample was determined utilizing the following equation.

$$v_e = E'/3RT \quad (1)$$

In the equation, E' represents the storage modulus energy (G') at a temperature $T_g + 30 \text{ }^\circ\text{C}$, while R stands for the universal gas constant ($8.314 \text{ J}\cdot\text{mol}^{-1}\cdot\text{K}^{-1}$), and T denotes the absolute temperature corresponding to $T_g + 30 \text{ }^\circ\text{C}$. The results of the storage modulus at $25 \text{ }^\circ\text{C}$ (G'_{25}) and v_e of the EWOMA-HEMA resins were shown in Table S3.

Mechanical property testing was conducted using an AG-20I electronic universal testing machine (Shimadzu, Tokyo, Japan) at a stretching rate of $5 \text{ mm}/\text{min}$. The test specimens were 3D printed as 1BA dumbbell-shaped specimens following the guidelines outlined in China Standard GB/T 1040.2-2006 [78]. The viscosity of the WCO-based coating was tested with an NDJ-8s viscometer (Jitai, Shanghai, China). The pencil hardness of the coating film was examined using a QHQ-A pencil hardness tester (Sanhe, Dongguan,

China) according to the China Standard GB/T 6739-2006 [79]. The adhesion of the coating film was tested using a QFH film adhesion tester (Sanhe, Dongguan, China) according to the China Standard GB/T 9286-1998 [80]. The impact strength of the coating film was measured with a QCJ film impact tester (Sanhe, Dongguan, China) according to the China Standard GB/T 1732-2020 [81]. The water resistance and alcohol resistance of the paint film were tested according to the China Standards GB/T 5209-1985 [82] and GB/T 1763-1979 [83], respectively. The gloss measurement was conducted in accordance with China Standard GB/T 9754-2007 [84] using a YG 60 gloss meter (Sanenshi, Shenzhen, China) with a measuring angle of 60°. Yellow index testing was performed according to China Standard 23983-2009 [85] using a ZYLH-UV3A40 UV climate resistance test chamber (Lihua, Suzhou, China). Additionally, the degree of yellowing (ΔE) of the coating was assessed using a BGD 555 colorimeter (Shenyuan, Zibo, China).

The contact angle of the WCO-based coating was measured using a JGW-360A contact angle meter (Chongda, Xiamen, China) to assess the surface wettability. To assess the antismudge properties of the WCO-based coatings, the following procedure was employed: After curing, the coatings were allowed to sit at room temperature for 8 h, with an uncoated tinplate serving as a control. Subsequently, a water-based marker pen was utilized to draw lines on the coating surface at a rate of 4 cm/s. A photograph was taken once the ink on the coating surface ceased to shrink. Any remaining ink residue on the coating surface was gently removed using a soft cloth. The area of the ink trace left on the coating surface after ink shrinkage was quantified using ImageJ 2.0.0-rc-69 software [86–89]. The anticorrosion performance of the WCO-based coating was evaluated by immersing the coated tinplates in a brine solution (5.0 wt% NaCl aqueous solution). An uncoated tinplate served as a control. The corrosion condition was periodically monitored, and the coating's resistance to corrosion was assessed based on visible changes, such as rusting, discoloration, or coating peeling.

3. Results and Discussion

3.1. Photocurable Behavior

The photocurable behavior of the liquid EWOMA-HEMA (A3 sample) and pure EWOMA coating was investigated using the P-DSC method. As depicted in Figure 2a,b, the coating containing only EWOMA and TPO (initiator) could still undergo curing when exposed to 405 nm purple light, even in the absence of HEMA. However, the curing rate was relatively slow, requiring 90 and 189 s to reach 60% and 80% of the ultimate conversion, respectively. The introduction of HEMA effectively enhanced the photopolymerizable reaction. For instance, the EWOMA-HEMA coating with a mass ratio of EWOMA to HEMA at 4:1 (A3 sample) only required 22 and 98 s to reach 60% and 80% of the ultimate conversion, respectively, thereby better suiting the requirements of high-efficiency coating production. In the course of the actual photocuring process for the coating film, the viscosity of liquid EWOMA-HEMA (A3 sample) underwent a substantial increase within 30 s of light exposure. By the 50-s mark, its viscosity had surged to 6237 MPa·s, nearly nine times that of the initial sample (681 MPa·s). Following this, it swiftly lost its fluidic properties, leading to the formation of a solid coating film (refer to Figure S2 in ESI).

3.2. Structural Characterization

The IR spectra for the liquid EWOMA-HEMA (A3 sample) and its cured coating film are presented in Figure 3a. The liquid WCO-based coating exhibited distinct absorption peaks associated with the unsaturated bonds present in EWOMA and HEMA, including C=C stretching vibration (1637 cm^{-1}), in-plane and out-of-plane bending vibrations of =CH₂ (1403 cm^{-1} and 943 cm^{-1} , respectively), as well as in-plane and out-of-plane bending vibrations of -CH= (1295 cm^{-1} and 813 cm^{-1} , respectively). In the cured coating film, all the previously mentioned absorption peaks related to unsaturated bonds either disappeared or significantly weakened. This observation indicates that the light-curing process of the

WCO-based coating primarily involves the polymerization of the C=C double bonds within EWOMA and HEMA.

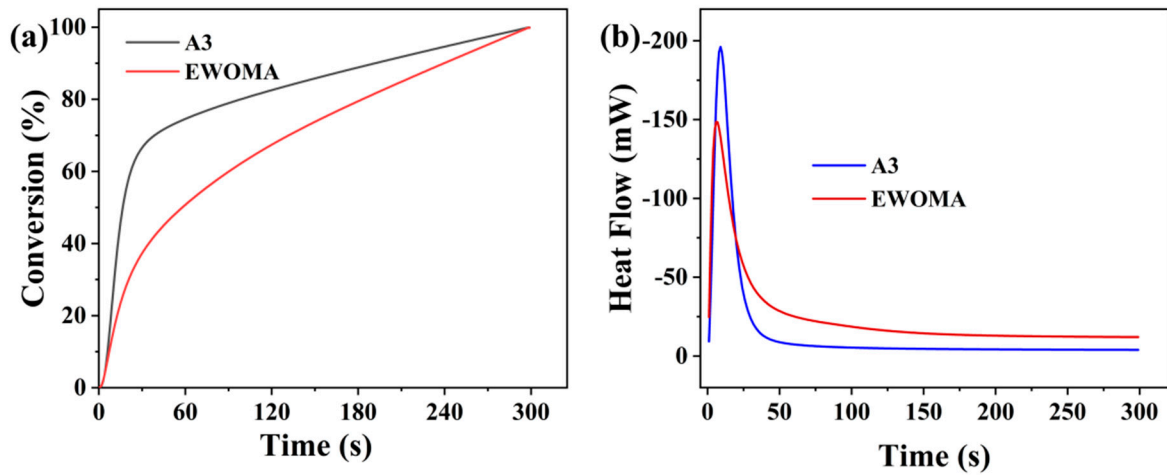


Figure 2. The photopolymerisable conversions (a) and P-DSC curves (b) of pure EWOMA and EWOMA-HEMA resin (A3 sample).

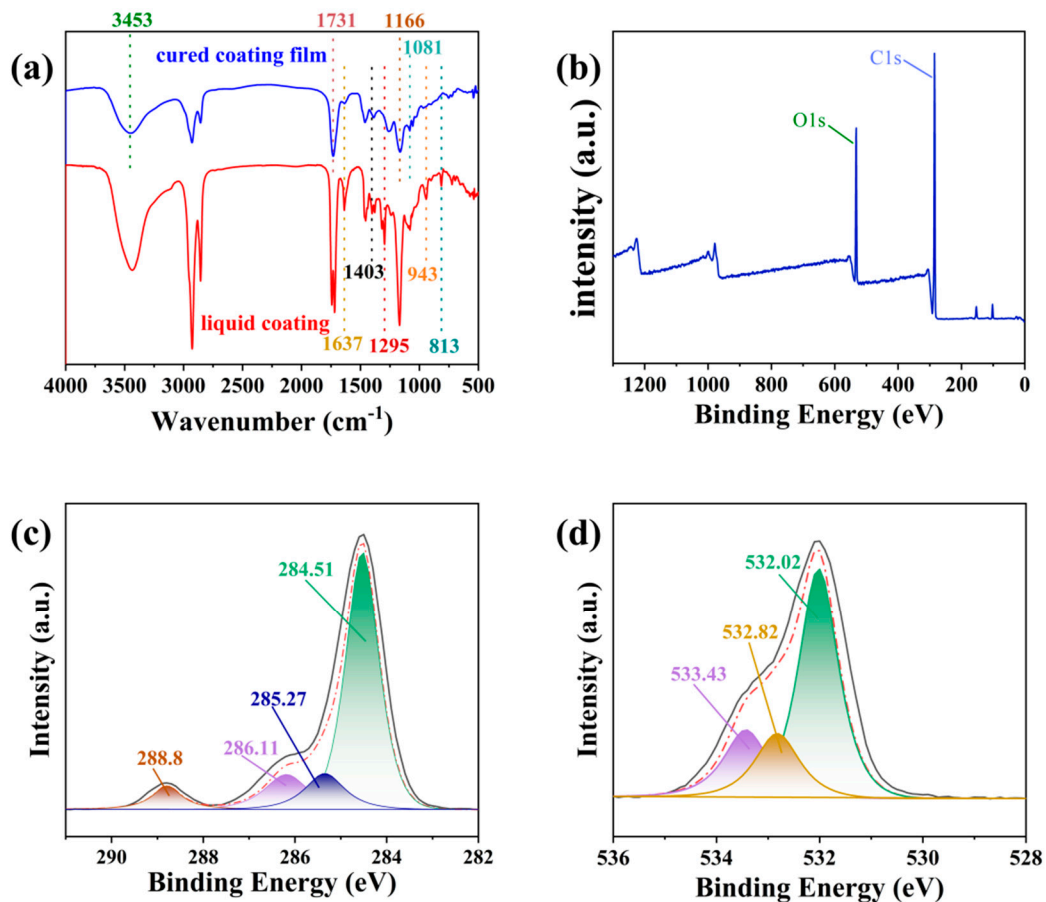


Figure 3. (a) IR spectra of liquid and cured coating film of EWOMA-HEMA resin; (b–d) The full XPS (b), C1s (c) and O1s (d) high-resolution spectra of cured EWOMA-HEMA resin.

Both the IR and XPS spectra of the cured EWOMA-HEMA resin revealed the presence of various lateral functional groups within its polymeric network, encompassing hydroxyl and carboxylate groups. In the IR spectrum of cured A3 resin (refer to Figure 3a), a broad

peak centered at 3434 cm^{-1} was observed, which likely corresponds to the stretching vibrations of O–H in the hydroxyl groups, while the peaks at 1166 and 1081 cm^{-1} could be due to the vibrations of C–O bonds connecting the hydroxyl groups. The stretching vibration of the C=O bond in the carboxylate group was located at 1731 cm^{-1} . The existence of hydroxyl and carboxylate groups was also proven by the XPS spectra of the cured coating film (see Figure 3b–d). In the high-resolution spectrum of C1s, the characteristic peaks at 284.51 eV, 285.27 eV, 286.11 eV, and 288.8 eV could be attributed to the C–C bond, C–O bond in the hydroxyl group, C=O bond in the carboxylate group, and –COOH in the carboxyl group, respectively (see Figure 3c). The high-resolution spectra of O1s also exhibited the existence of the carboxylate group, carboxyl group and hydroxyl group, whose characteristic signals were located at 532.02 eV, 532.82 eV, and 533.43 eV, respectively (see Figure 3d). Considering the insights from the IR spectrum, it became evident that the cured coating film composed of EWOMA-HEMA resin formed a crosslinked polymeric network, with contributions from both WCO and HEMA segments.

3.3. Thermal Analysis

Dynamic mechanical analysis was conducted on the cured EWOMA-HEMA coatings, and the outcomes are presented in Figure 4 and Table S3. It was observed that the storage modulus at room temperature (G'_{25}) initially increased and subsequently decreased as the HEMA dosage increased. Remarkably, the EWOMA-HEMA coating with a mass ratio of EWOMA to HEMA at 4:1 (A3 sample) exhibited the highest storage modulus at room temperature (564.1 MPa). Alongside the rise in HEMA amount, the crosslinking density (v_c) exhibited comparable trends with G'_{25} , with an initial increase followed by a decrease. Upon reaching a mass ratio of EWOMA to HEMA of 4:1 (Sample A3) in the cured coating, the highest crosslinking density was obtained ($1.22 \times 10^{-2}\text{ mol/cm}^3$), indicating the possibility of better mechanical properties and facilitating the development of high-quality coatings. Furthermore, similar to other WCO-based resins reported previously, the cured WCO-based coating demonstrated exceptional thermal stability. The TGA results indicated that the cured product of EWOMA-HEMA resin could withstand temperatures of up to $280\text{ }^\circ\text{C}$, eventually leading to thermal decomposition at approximately $500\text{ }^\circ\text{C}$ (see Figure S3 and Table S3 in ESI). Additionally, the DSC results revealed a distinctive pattern in the glass transition temperature (T_g) values of the cured EWOMA-HEMA coatings. Initially, T_g values exhibited an ascending trend, only to be followed by a subsequent decline, specifically within the mass ratio range of EWOMA to HEMA from 3:1 to 6:1 (represented by samples A2 to A6). Of noteworthy significance, sample A3, characterized by the highest cross-linking density, prominently displayed the peak T_g value of $35.38\text{ }^\circ\text{C}$. However, a captivating anomaly surfaced in the case of sample A1, which bore the highest HEMA content at a mass ratio of EWOMA to HEMA of 2:1. Paradoxically, despite possessing the lowest cross-linking density, this sample exhibited the highest T_g value of $42.23\text{ }^\circ\text{C}$. This intriguing phenomenon might be ascribed to the presence of a larger proportion of HEMA monomers within the polymer system. This condition prompted the HEMA monomers to undergo a distinct polymerization process, separate from the EWOMA-HEMA cross-linking network. As a result, the self-polymerized HEMA segments demonstrated limited contribution to the cross-linking network. However, their presence effectively restricted the segmental mobility within the overall cross-linking structure, thereby significantly enhancing the observed T_g value (as illustrated in Figure S4 and Table S3 in ESI).

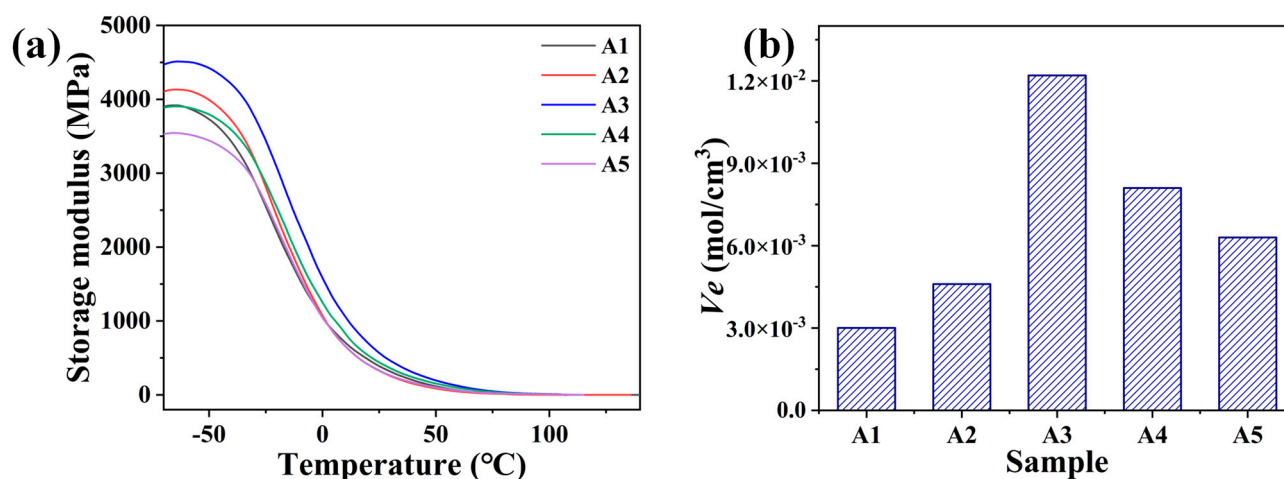


Figure 4. The storage modulus (a) and cross-linking density (b) of EWOMA-HEMA coatings with different dosages of HEMA.

3.4. Mechanical Property

A good coating requires a matrix resin with favorable mechanical properties. As depicted in Figure 5a and Figure S5 in ESI, the cured resin made solely from EWOMA demonstrated weak mechanical characteristics, with a tensile strength of 0.19 MPa and a breaking elongation of 5.76%. Such properties would significantly compromise the quality of the coating. However, by introducing HEMA as a second monomer, the mechanical properties of the resins based on WCO could be significantly improved, particularly the tensile strength. Similarly to the trend observed in cross-linking density, the mechanical properties of the EWOMA-HEMA resins generally increased initially with the addition of HEMA but then decreased. The EWOMA-HEMA resin formulated with the optimal recipe (A3 sample, where EWOMA:HEMA = 4:1 by mass) exhibited hardness and toughness, with a good tensile strength of 9.29 MPa and a favorable elongation at break of 38.1%. These values were 48 and 6 times higher than those of pure EWOMA, respectively. Building upon our previous studies [22], this further validates that introducing an appropriate second monomer is a crucial step in producing practical WCO-based photocurable resins. As illustrated in Figure 5b and Table S4 in ESI, in comparison to other SO-based photocurable resins for coatings [90–94]. The resulting WCO-based photocurable resin displayed comparable mechanical strength and could serve as a sustainable alternative with reduced cost and enhanced environmental friendliness.

3.5. Coating Properties

The physical properties of the EWOMA-HEMA coatings, including viscosity, pencil hardness, adhesion, impact strength, water resistance, gloss and yellowing index, were evaluated and presented in Table 2. Pure EWOMA exhibited a very high viscosity of 4321 MPa·s, which could make it challenging to achieve smooth coating films. Moreover, the pure EWOMA coating demonstrated weak performance in terms of pencil hardness (6B), adhesion (Grade 4), and impact strength (1 kg/cm) due to their weak mechanical properties. Additionally, the pure EWOMA coating displayed a generally moderate level of glossiness (94) and demonstrated inadequate resistance to yellowing. Following a 96-h exposure to ultraviolet light, its yellowing value (ΔE) increased to 4.36. Therefore, without the addition of a second monomer, pure EWOMA is not suitable for practical coating applications.

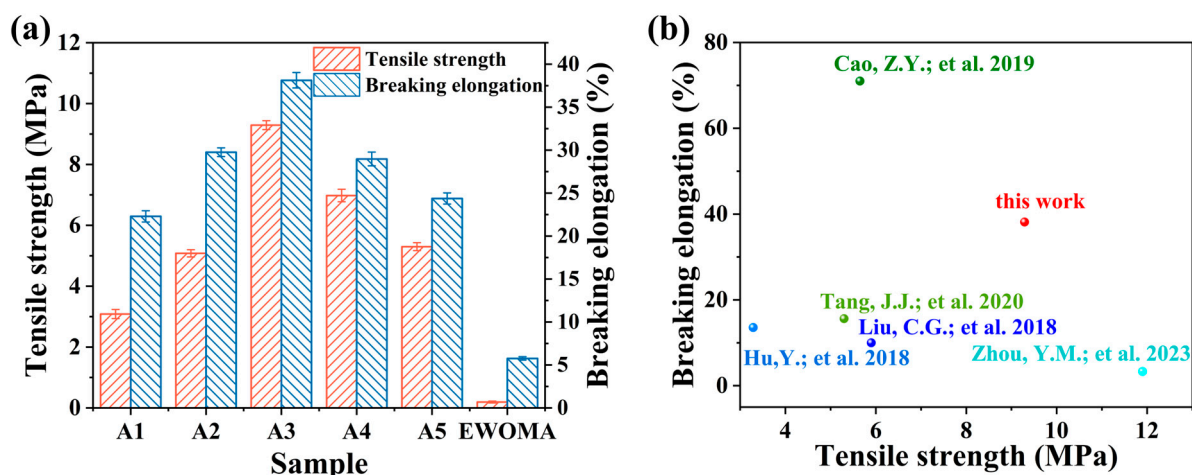


Figure 5. (a) Tensile property test of pure EWOMA and EWOMA-HEMA resins with different dosages of HEMA; (b) The comparison of the mechanical properties of the resulting WCO-based resin (A3 sample) with those of other photocurable coatings derived from vegetable oils ([90–94], this work).

Table 2. The coating performance of pure EWOMA and EWOMA-HEMA coatings with different dosages of HEMA.

Sample	Viscosity (MPa·s)	Pencil Hardness	Adhesion (Grade)	Impact Strength (kg/cm)	Water Resistance (24 °C, 96 h)	Gloss °60 (GU)	Yellowing Index (ΔE, 96 h)
A1	207	2B	4	33	Small amount of tiny bubbles	101.6	0.27
A2	433	B	3	38	Small amount of tiny bubbles	103.7	0.29
A3	681	2H	2	62	No significant change	110.7	0.24
A4	1039	B	3	23	No significant change	104.4	0.43
A5	1628	B	4	18	No significant change	102.3	0.46
EWOMA	4321	6B	4	1	Small amount of tiny bubbles	94	4.36

However, by incorporating an appropriate amount of HEMA as a second monomer, the viscosity of the liquid coating decreased, improving its flowability and facilitating the application process. For instance, the viscosity of the A3 sample was only 15.8% of that of pure EWOMA. Furthermore, the addition of HEMA significantly enhanced the performance of the cured coating film in various aspects. Similar to the trend observed in mechanical strength variation, the WCO-based coating formulated with the optimal recipe (A3 sample, where EWOMA:HEMA = 4:1 by mass) exhibited the best coating properties. It demonstrated good pencil hardness (2H), excellent adhesion (Grade 2), outstanding impact strength (62 kg/cm, three times higher than that of pure EWOMA), and good water resistance. Additionally, it has been observed that the introduction of HEMA as a secondary monomer brings about a marginal enhancement in the film's glossiness while notably elevating the coating's capacity to resist yellowing. For instance, in the case of sample A3, the gloss value surged to 110.7, while after undergoing a 96-h exposure to ultraviolet light, the yellowing value was a mere 0.24. These substantial improvements markedly outperform the attributes of the pure EWOMA coating. Compared to other SO-based photocurable coatings [91–93,95–98], the resulting WCO-based coating (A3 sample) also showed comparable properties, making it a practical, environmentally friendly, and cost-effective, sustainable coating option (see Table 3).

Table 3. The comparison of coating performance between the resulted in WCO-based coating (A3 sample) and another vegetable oil-based photocurable coating.

Serial Number	Major Compositions	Pencil Hardness	Adhesion (Grade)	References
1	Epoxidized soybean oil (ESO) Hydroxyethyl methacrylated maleate (HEMAMA)	HB	3	[96]
2	Acrylated epoxidized soybean oil (AESO) Hydroxyethyl methacrylate (HEMA)	2H	2	[92]
3	Epoxidized rose hip seed oil (ERHO)	B	2	[95]
4	Epoxidized grape-seed oil (EGRP) Dimethylolpropionic acid (DMPA)	B	3	
5	Methacrylic anhydride (MAAH) 4-Dimethylaminopyridine (DMAP) Trimethylol-propane triacrylate (TMPTA)	H	2	[91]
6	Epoxidized soybean oil (AESO) Castor oil (CO) Pentaerythritol (PER) Acryloyl chloride (AC)	4B	2	[93]
7	Epoxidized soybean oil (ESO) 3,4-epoxycyclohexylmethyl-3,4- epoxycyclohexanecarboxylate (UVR 6110) 4-Thiophenyl phenyl diphenyl sulfonium hexafluoroantimonate (UVI 6974) Trifunctional primary ϵ -caprolactone triol (Tone Polyol 0305)	H	0	[97]
8	thioglycerol modified castor oil (TCO) Isophorone diisocyanate (IPDI)	4H	2	[98]
9	Epoxy waste oil methacrylate (EWOMA) Hydroxyethyl methacrylate (HEMA)	2H	2	This work

3.6. Antismudge Property

Generally, ink from a marker pen is difficult to shrink and erase on a regular object's surface. However, when applied to a coating surface with antismudge properties, the ink can shrink after writing, allowing for easy wiping on the coated surface. In this study, water-based markers were used to write on four types of coatings: WCO-based coatings (samples A1, A3 and A5) and pure EWOMA. The extent of ink shrinkage was analyzed using ImageJ software, which calculated the percentage of ink residual area after shrinkage. Additionally, the smudge resistance was evaluated by determining whether the ink trace could be cleaned using a dust-free soft wipe.

As depicted in Figure 6, uncoated tinplate consistently left behind thick and persistent ink traces without any shrinkage, resulting in an ink residual area that could reach almost 100%. Moreover, these ink traces were difficult to remove by wiping, indicating the absence of antismudge properties in uncoated tinplate. Pure EWOMA coating exhibited moderate resistance to smudging, as the ink shrank to some extent on its surface, leading to a reduction in the ink residual area to 24.4%. However, complete removal of the ink residue from the pure EWOMA coating was not possible through wiping alone. In contrast, the A3 sample demonstrated superior antismudge properties, exhibiting a significantly lower ink residual area of 6.8%. The ink residue on the A3 coating could be effortlessly and entirely removed by wiping. It was also observed that with an increase in the HEMA content, its antismudge properties showed a slight improvement. When the mass ratio of EWOMA to HEMA decreased from 6:1 to 2:1, the ink residual area decreased from 11.5% to 5.7%. Furthermore, the study observed that the smudge resistance was linked to the hydrophobicity of the material. As shown in Figure S6 in ESI, the pure EWOMA coating displayed relatively strong hydrophilicity with a contact angle of 66.8°. The introduction of HEMA increased the surface hydrophobicity of the coating, potentially due to its ability to form internal hydrogen bonds, thereby reducing the presence of surface hydroxyl groups. Consequently, the hydrophobic surface of the EWOMA-HEMA coating, such as the A3 coating with a water contact angle of 93.6°, exhibited lower surface energy compared to pure EWOMA, which could contribute to its good antismudge performance.

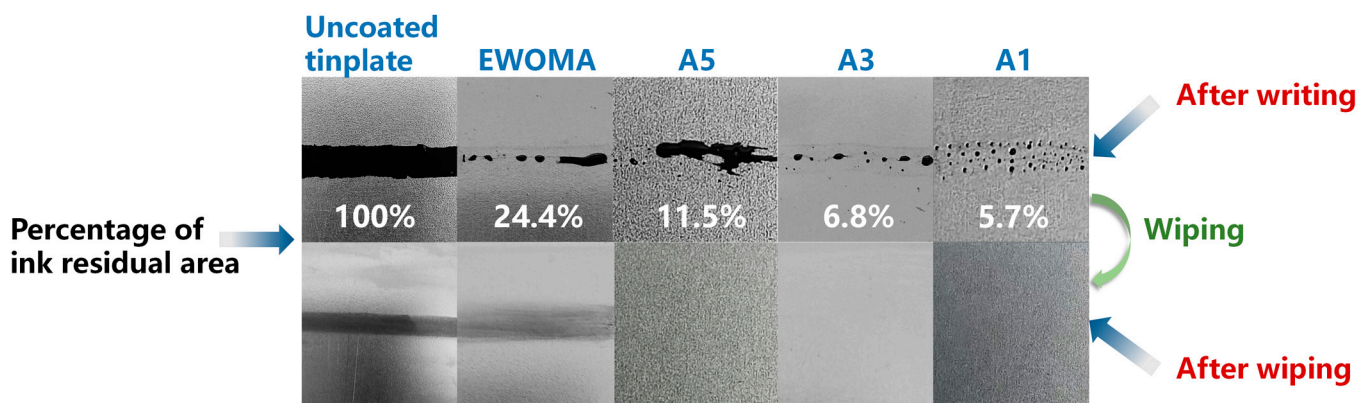


Figure 6. Optical photos of ink trace remained by a water-based marker on uncoated tinplate, pure EWOMA, A1, A3 and A5 photocurable coatings. The ink residual trace was cleaned with a dust-free wipe after ink shrinkage. The percentage of the ink residual trace area was labeled.

3.7. Anticorrosive Property

As depicted in Figure 7, the anticorrosion performance of the WCO-based coating (A3 sample and pure EWOMA) was assessed by immersing the coatings applied to the tinplate in a brine solution. Corrosion resistance was evaluated based on macroscopic observations. It was observed that the uncoated tinplate exhibited poor corrosion resistance, with noticeable signs of rust appearing after five days and severe corrosion of the entire tinplate after 20 days. Although the pure EWOMA coating provided a certain level of protection to the tinplate, it was unable to prevent corrosion after 20 days due to its relatively weak adhesion in the brine environment. The pure EWOMA coating started foaming after five days, exhibited significant foaming after 10 days, and gradually peeled off after 15 days, thereby failing to completely isolate the external air and moisture. In contrast, the EWOMA-HEMA coating (A3 sample) remained intact throughout the 20-day period, indicating much stronger adhesion compared to the pure EWOMA coating, effectively preventing corrosion and rusting of the tinplate.



Figure 7. Optical photos with different surface corrosive results of uncoated tinplate, pure EWOMA and EWOMA-HEMA resin (A3 sample) coated on tinplate submerged in 5.0 wt% NaCl solution for different times.

3.8. Aldehyde Content

Due to repeated heating and frying, the WCO contains a variety of hazardous organic compounds. Among these, aldehydes are the main volatile organic chemicals present in WCO, which can stimulate the mucosa, corrode the skin, and even potentially cause cancer [99–103]. As depicted in Figure 8, the WCO used in this study exhibited a significantly high aldehyde content of $18.83 \mu\text{g}\cdot\text{g}^{-1}$, resulting in a noticeable rancid odor. However, by employing the “epoxidation & ring-opening esterification” method, the malodorous aldehydes could be effectively eliminated. The coating of EWOMA-HEMA (A3 sample) demonstrated a remarkably low aldehyde content ($0.34 \mu\text{g}\cdot\text{g}^{-1}$), which was only 1.8% of that of WCO, thus ensuring the safety and well-being of consumers.

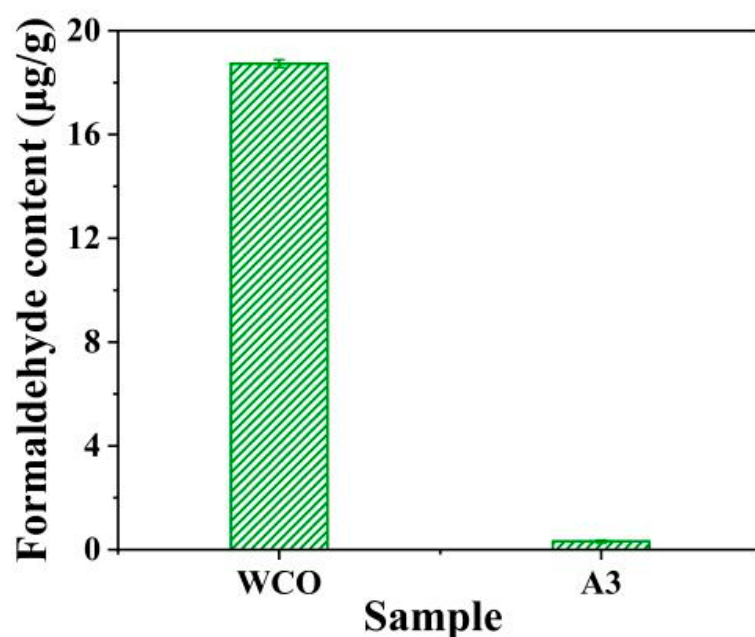


Figure 8. The aldehyde content of WCO as raw material and WCO-based coating (A3 sample).

4. Conclusions

This study explores the synthesis and characteristics of a photocurable coating formulated with WCO as the primary ingredient. The findings affirm that employing the “epoxidation & ring-opening esterification” method for generating photocurable monomers from WCO, in conjunction with the inclusion of HEMA as a secondary monomer, effectively mitigates several drawbacks associated with WCO. As a result, a practical WCO-based coating is successfully developed for the first time. The cured coating, optimized with a composition of EWOMA: HEMA in a mass ratio of 4:1, exhibits several advantageous characteristics, including low viscosity, excellent adhesion, high pencil hardness, exceptional impact strength, nice glossiness and resistance to yellowing, good resistance to smudging, effective corrosion protection, and low aldehyde content. These qualities make it an environmentally friendly, cost-effective, and sustainable coating option.

Considering catering waste recycling, the resulting WCO-based coating presents a range of advantages. It features a straightforward synthesis process, operates under gentle reaction conditions, follows a convenient synthesis route, avoids secondary pollution, maintains low synthesis costs, and boasts a high product profit margin. Consequently, it effectively tackles the existing issues related to the low added value and restricted market competitiveness of recycled WCO products. This research, therefore, presents favorable commercial opportunities and introduces a novel approach to WCO recycling.

Supplementary Materials: The following supporting information can be downloaded at: <https://www.mdpi.com/article/10.3390/coatings13091553/s1>, Figure S1: The absorption spectrum of the WCO-based photocurable coating and the emission spectrum of the LCD curing light sources; Figure S2: Viscosity changes of liquid EWOMA-HEMA at various irradiation time intervals; Figure S3: TGA and DTG curves of EWOMA-HEMA coatings with different dosages of HEMA; Figure S4: DSC curves of EWOMA-HEMA coatings with different dosages of HEMA and the value of T_g of A1–A5 samples; Figure S5: Stress-strain curves of pure EWOMA and EWOMA-HEMA coatings with different dosages of HEMA; Figure S6: Water contact angle of pure EWOMA and EWOMA-HEMA coatings with different dosages of HEMA; Figure S7: The cross cut picture of EWOMA-HEMA coatings; Table S1: Fatty acid compositions (wt.%) of five kinds of oil; Table S2: The Lovibond color codes of WCO and E-WCO; Table S3: DMA, DSC and TGA results of the WCO-based coatings; Table S4: The comparison of mechanical properties between the resulted WCO-based resin and other vegetable oil-based photocurable coating.

Author Contributions: Conceptualization, methodology & writing (original draft preparation): M.L.; Software: Y.L.; Investigation: P.W. and W.Y.; Resources & Data curation: Q.L.; Formal Analysis: G.D.; Writing (review and editing), project administration, funding acquisition & supervision: S.C. All authors have read and agreed to the published version of the manuscript.

Funding: This work was supported by grants from the National Nature Science Foundation of China (No. 51763007) and the Guangxi Natural Science Foundation Program (No. 2015GXNSFBA139033).

Institutional Review Board Statement: Not applicable.

Informed Consent Statement: Not applicable.

Data Availability Statement: Not applicable.

Conflicts of Interest: The authors declare no conflict of interest.

Abbreviations

WCO	Waste cooking oil
EWOMA	Epoxy waste oil methacrylate
HEMA	2-hydroxyethyl methacrylate
MAA	Methacrylic acid
TPO	2,4,6-trimethylbenzoyldiphenyl phosphine oxide
PPh ₃	Triphenylphosphine
HQ	Hydroquinone

Symbols

A1–A5	WCO-based coating samples with different dosages of HEMA
-------	--

References

1. Landi, F.F.A.; Fabiani, C.; Castellani, B.; Cotana, F.; Pisello, A.L. Environmental assessment of four waste cooking oil valorization pathways. *Waste Manag.* **2022**, *138*, 219–233. [[CrossRef](#)] [[PubMed](#)]
2. Manikandan, G.; Kanna, P.R.; Taler, D.; Sobota, T. Review of Waste Cooking Oil (WCO) as a Feedstock for Biofuel-Indian Perspective. *Energies* **2023**, *16*, 1739. [[CrossRef](#)]
3. Bandbafha, H.H.; Li, C.; Chen, X.M.; Peng, W.X.; Aghbashlo, M.; Lam, S.S.; Tabatabaei, M. Managing the hazardous waste cooking oil by conversion into bioenergy through the application of waste-derived green catalysts: A review. *J. Hazard. Mater.* **2022**, *424*, 127636. [[CrossRef](#)]
4. Kulkarni, M.G.; Dalai, A.K. Waste Cooking Oils An Economical Source for Biodiesel: A Review. *Ind. Eng. Chem. Res.* **2006**, *45*, 2901–2913. [[CrossRef](#)]
5. Foo, W.H.; Chia, W.Y.; Tang, D.Y.Y.; Koay, S.S.N.; Lim, S.S.; Chew, K.W. The conundrum of waste cooking oil: Transforming hazard into energy. *J. Hazard. Mater.* **2021**, *47*, 126129. [[CrossRef](#)]
6. Andrew, N.A.; Nelson, I.E.; Obahiagbon, K. Optimum biodiesel production from waste vegetable oil using functionalized cow horn catalyst: A comparative evaluation of some expert systems. *Clean. Eng. Technol.* **2021**, *4*, 100184.
7. Kamel, D.A.; Farag, H.A.; Amin, N.K.; Zatout, A.A.; Fouad, Y.O. Optimum biodiesel production from waste vegetable oil using functionalized cow horn catalyst: A comparative evaluation of some expert systems. *Environ. Sci. Pollut. Res.* **2019**, *26*, 32804–32814. [[CrossRef](#)]
8. Wang, E.P.; Ma, X.; Tang, S.Z.; Yan, R.; Wang, Y.; Riley, W.W.; Reaney, M.J.T. Synthesis and oxidative stability of trimethylolpropane fatty acid triester as a biolubricant base oil from waste cooking oil. *Sci. Direct* **2014**, *175*, 371–378. [[CrossRef](#)]

9. Cai, Z.Z.; Zhuang, X.C.; Yang, X.H.; Huang, F.R.; Wang, Y.; Li, Y. Litsea cubeba kernel oil as a promising new medium-chain saturated fatty acid feedstock for biolubricant base oil synthesis. *Ind. Crops Prod.* **2021**, *167*, 113564. [[CrossRef](#)]
10. Hussein, R.Z.K.; Attia, N.K.; Fouad, M.K.; ElSheltawy, S.T. Experimental investigation and process simulation of biolubricant production from waste cooking oil. *Biomass Bioenergy* **2021**, *144*, 105850. [[CrossRef](#)]
11. Chen, C.Y.; Li, D.S.; Suna, N.; Ma, X.F.; Xiao, G.Q.; Zhou, J. Oil recovery from drilling cuttings by biosurfactant from kitchen waste oil. *Energy Sources* **2021**, *43*, 314–325. [[CrossRef](#)]
12. Kurt, I.; Acar, I.; Güclü, G. Preparation and characterization of water reducible alkyd resin/colloidal silica nanocomposite coatings. *Prog. Org. Coat.* **2014**, *77*, 949–956. [[CrossRef](#)]
13. Ma'nczyk, K.; Szewczyk, P. Highly branched high solids alkyd resins. *Prog. Org. Coat.* **2002**, *44*, 99–109. [[CrossRef](#)]
14. Ifijen, I.H.; Odi, H.D.; Maliki, M.; Omorogbe, S.O.; Aigbodion, A.I.; Ikhuoria, E.U. Correlative studies on the properties of rubber seed and soybean oil-based alkyd resins and their blends. *J. Coat. Technol. Res.* **2021**, *18*, 459–467. [[CrossRef](#)]
15. Milhem, S.A.; Verrielle, M.; Nicolas, M.; Thevenet, F. Indoor use of essential oil-based cleaning products: Emission rate and indoor air quality impact assessment based on a realistic application methodology. *Atmos. Environ.* **2021**, *246*, 118060. [[CrossRef](#)]
16. Patil, P.D.; Buradkar, A.M.; Mulla, M.Z.; Prabhu, P.A.; Nagla, J.R. Taguchi Optimization for Waste Cooking Oil Based Biodiesel Preparation. *Int. J. Eng. Adv. Technol.* **2020**, *9*, 1088–1097. [[CrossRef](#)]
17. Xiao, M.S.; Lin, D.R.; Li, Z.H.; Zhao, J.J.; Long, X.M.; Wu, Z.J. Synthesis of Biodiesel from Waste Cooking Oil by One-step Esterification and Its Structural Characterization. *Waste Biomass Valorization* **2020**, *11*, 2087–2100. [[CrossRef](#)]
18. Mohadesi, M.; Aghel, B.; Maleki, M.; Ansari, A. Study of the transesterification of waste cooking oil for the production of biodiesel in a microreactor pilot: The effect of acetone as the co-solvent. *Fuel* **2020**, *273*, 117736. [[CrossRef](#)]
19. Das, S.; Das, B.; Misra, R.D. Emergy-based assessment of biodiesel production in India using edible and non-edible oil. *Int. J. Environ. Sci. Technol.* **2022**, *19*, 11117–11144. [[CrossRef](#)]
20. Alkhafaje, Z.A.; Mohammed, A.K.; Rashid, I.M. Development of two-step noncatalytic esterification of waste cooking oil for biodiesel preparation. *Mech. Catal.* **2020**, *131*, 645–659. [[CrossRef](#)]
21. Demirbas, A.; Bafail, A.; Ahmad, W.; Sheikh, M. Biodiesel production from non-edible plant oils. *Energy Explor. Exploit.* **2016**, *34*, 290–318. [[CrossRef](#)]
22. Liu, Y.; Liu, M.Y.; Fan, X.G.; Wang, L.; Liang, J.Y.; Jin, X.Y.; Che, R.J.; Ying, W.Y.; Chen, S.P. Four-Dimensional Printing of Multifunctional Photocurable Resin Based on Waste Cooking Oil. *ACS Sustain. Chem. Eng.* **2022**, *10*, 16344–16358. [[CrossRef](#)]
23. Liu, Y.; Liu, M.Y.; Qi, Y.X.; Jin, X.Y.; Xu, H.R.; Chen, Y.X.; Chen, S.P.; Su, H.P. Synthesis and properties of wax based on waste cooking oil. *RSC Adv.* **2022**, *12*, 3365–3371. [[CrossRef](#)] [[PubMed](#)]
24. Liu, Y.; Fan, X.G.; Liu, M.Y.; Wang, L.; Wang, P.Y.; Xu, H.R.; Chen, Y.X.; Chen, S.P. Fatty acid wax from epoxidation and hydrolysis treatments of waste cooking oil: Synthesis and properties. *RSC Adv.* **2022**, *12*, 36018–36027. [[CrossRef](#)]
25. Xiong, Y.; Miao, W.F.; Wang, N.N.; Chen, H.M.; Wang, X.R.; Wang, J.Y.; Tan, Q.L.; Chen, S.P. Solid alcohol based on waste cooking oil: Synthesis, properties, micromorphology and simultaneous synthesis of biodiesel. *Waste Manag.* **2019**, *85*, 295–303. [[CrossRef](#)]
26. Zhang, Y.N.; Sheng, Y.M.; Wang, M.H.; Lu, X. UV-curable self-healing, high hardness and transparent polyurethane acrylate coating based on dynamic bonds and modified nano-silica. *Prog. Org. Coat.* **2022**, *172*, 107051. [[CrossRef](#)]
27. Jovičić, M.; Radičević, R.; Pavličević, J.; Bera, O.; Govedarica, D. Synthesis and characterization of ricinoleic acid based hyper-branched alkyds for coating application. *Prog. Org. Coat.* **2020**, *148*, 105832. [[CrossRef](#)]
28. Huang, J.; Zhang, J.S.; Zhu, G.Q.; Yu, X.X.; Hu, Y.; Shang, Q.Q.; Cheng, J.Q.; Hu, L.H.; Zhou, Y.H.; Liu, C.G. Self-healing, high-performance, and high-biobased-content UV-curable coatings derived from rubber seed oil and itaconic acid. *Prog. Org. Coat.* **2021**, *159*, 106391. [[CrossRef](#)]
29. Ang, D.T.C.; Gan, S.N. Development of palm oil-based alkyds as UV curable coatings. *Pigment Resin Technol.* **2012**, *41*, 302–310.
30. Mishra, V.; Mohanty, I.; Patel, M.R.; Patel, K.I. Development of Green Waterborne UV-Curable Castor Oil-Based Urethane Acrylate Coatings: Preparation and Property Analysis. *Int. J. Polym. Anal. Charact.* **2015**, *20*, 504–513. [[CrossRef](#)]
31. Yu, X.X.; Hu, Y.; Lei, W.; Liu, C.G.; Zhou, Y.H. Development of Catalyst-Free Self-Healing Biobased UV-Curable Coatings via Maleate Monoester Transesterification. *Coatings* **2023**, *13*, 110. [[CrossRef](#)]
32. Bashkirova, K.A.; Gazeev, M.V.; Sviridov, A.V. Features of planning an experiment to develop a new paint and varnish composition for the formation of protective and decorative coatings on wood products. *IOP Conf. Ser. Earth Environ. Sci.* **2022**, *949*, 012065. [[CrossRef](#)]
33. Jeon, M.; Cho, B.R.; Han, M.; Lee, C.; Yoon, S.C. Synthesis of Photocurable Fluorenylidene Diacrylate for Optical Application. *Mol. Cryst. Liq. Cryst.* **2008**, *492*, 303–311. [[CrossRef](#)]
34. Ortiz, R.A.; Padilla, E.E.G.; Valdez, A.E.G.; Flores, R.A.; Muñoz, J.F.E. Development of a photocurable glass-fiber reinforced epoxy-amine/thiol-ene composite. *J. Polym. Res.* **2016**, *23*, 30. [[CrossRef](#)]
35. Sethayosongsa, R.; Chuayprakong, S.; Srisawadi, S.; Nuansing, W.; Chokevivat, W.; Methachan, B.; Srimongkol, S.; Suksanong, P. Multi-material additive manufacturing of MWCNT-based conductive photocurable resin and its antimicrobial property. *J. Mater. Res.* **2022**, *38*, 708–719. [[CrossRef](#)]
36. Wu, J.; Qian, Y.; Sutton, A.C.; Scala, J.J.L.; Webter, D.C.; Sibi, M.P. Bio-Based Furanic Di(meth)acrylates as Reactive Diluents for UV Curable Coatings: Synthesis and Coating Evaluation. *ACS Sustain. Chem. Eng.* **2021**, *9*, 15537–15544. [[CrossRef](#)]
37. Choi, W.C.; Lee, W.K.; Ha, C.S. Low-viscosity UV-curable polyurethane acrylates containing dendritic acrylates for coating metal sheets. *J. Coat. Technol. Res.* **2019**, *16*, 377–385. [[CrossRef](#)]

38. Chan, D.; Maikawa, C.L.; Aquino, A.I.; Raghavan, S.S.; Troxell, M.L.; Appel, E.A. Polyacrylamide-based hydrogel coatings improve biocompatibility of implanted pump device. *J. Biomed. Mater. Res.* **2023**, *111*, 910–920. [[CrossRef](#)]
39. Yeh, S.L.; Deval, P.; Tsai, W.B. Fabrication of Transparent PEGylated Antifouling Coatings via One-Step Pyrogallol Deposition. *Polymers* **2023**, *15*, 2731. [[CrossRef](#)]
40. Liu, M.; Tong, S.; Tong, Z.; Guan, Y.; Sun, Y. A strong, biodegradable and transparent cellulose-based bioplastic stemmed from waste paper. *J. Appl. Polym. Sci.* **2023**, *140*, e53671. [[CrossRef](#)]
41. Quan, Z.; Zhang, Q.; Li, H.; Sun, S.; Xu, Y. Fluorescent cellulose-based materials for information encryption and anti-counterfeiting. *Coord. Chem. Rev.* **2023**, *493*, 215287.
42. Yang, X.; Zhang, Y.; Ye, M.; Tang, Y.; Wen, Z.; Liu, X.; Li, C.C. Renewable lignin and its macromolecule derivatives: An emerging platform toward sustainable electrochemical energy storage. *Green Chem.* **2023**, *25*, 4154–4179.
43. Vasile, C.; Baican, M. Lignins as Promising Renewable Biopolymers and Bioactive Compounds for High-Performance Materials. *Polymers* **2023**, *15*, 3177.
44. Wang, Q.; Thomas, J.; Soucek, M.D. Investigation of UV-curable alkyd coating properties. *J. Coat. Technol. Res.* **2023**, *20*, 545–557. [[CrossRef](#)]
45. Lei, H.; Yao, N.; Wang, S.; Fang, X.; Wu, J.; Yang, G.; Hua, Z. Plant oil-based branched polymer coatings enhanced with nucleobases for achieving strong adhesion and outstanding environmental tolerance. *Chem. Eng. J.* **2023**, *471*, 144602. [[CrossRef](#)]
46. Shafranska, O.; Dahlgren, J.; Jones, A.; Tardiff, J.; Webster, D.C. Differing unsaturation levels of soybean oils impact the properties of peroxide-vulcanized carbon black-filled ethylene-propylene-diene monomer rubber. *J. Appl. Polym. Sci.* **2023**, *140*, e53872. [[CrossRef](#)]
47. Ma, Y.; Bei, Y.; Zhang, M.; Song, F.; Hu, F.; Kou, Z.; Hu, L.; Zhou, Y.; Jia, P. Synthesis of woody oil-based plasticizer via solvent-free Diels-Alder reaction and its biodegradability. *Ind. Crops Prod.* **2022**, *188*, 115646. [[CrossRef](#)]
48. Oktay, B.; Türkcän, J.H.; Özdemir, O.K.; Apohan, N.K. Vegetable oil-based epoxy coating materials for self-healing and anticorrosive applications. *Macromol. Res.* **2023**, *14*. [[CrossRef](#)]
49. Rosu, L.; Varganici, C.D.; Mustata, F.; Rosu, D.; Rosca, I.; Rusu, T. Epoxy Coatings Based on Modified Vegetable Oils for Wood Surface Protection against Fungal Degradation. *ACS Appl. Mater. Interfaces* **2020**, *12*, 14443–14458. [[CrossRef](#)]
50. Nepomuceno, N.C.; Fook, M.V.L.; Rives, A.; Mija, A.; Wellen, R.M.R. Bio-Based Epoxy Resins of Epoxidized Soybean oil Cured with Salicylic acid Loaded with Chitosan: Evaluation of Physical-Chemical Properties. *J. Polym. Environ.* **2023**, *31*, 2566–2575. [[CrossRef](#)]
51. Dinu, R.; Bejenari, I.; Volf, I.; Mija, A. Vegetable Oil-Based Resins Reinforced with Spruce Bark Powder and with Its Hydrochar Lignocellulosic Biomass. *Appl. Sci.* **2021**, *11*, 10649.
52. Mauro, C.D.; Genua, A.; Rymarczyk, M.; Dobbels, C.; Malburet, S.; Graillot, A.; Mija, A. Chemical and mechanical reprocessed resins and bio-composites based on five epoxidized vegetable oils thermosets reinforced with flax fibers or PLA woven. *Compos. Sci. Technol.* **2021**, *205*, 108678.
53. Thomas, J.; Nwosu, J.; Soucek, M.D. Sustainable biobased composites from norbornylized linseed oil and biomass sorghum fillers. *Compos. Commun.* **2023**, *42*, 101695. [[CrossRef](#)]
54. Miao, S.D.; Zhu, W.N.; Castro, J.; Nowicki, M.; Zhou, X.; Cui, H.T.; Fisher, J.P.; Zhang, L.J.G. 4D printing smart biomedical scaffolds with novel soybean oil epoxidized acrylate. *Sci. Rep.* **2016**, *6*, 27226.
55. Zhang, P.; Zhang, J. One-step acrylation of soybean oil (SO) for the preparation of SO-based macromonomers. *Green Chem.* **2013**, *15*, 641–645. [[CrossRef](#)]
56. Zhang, P.; Xin, J.; Zhang, J. Effects of Catalyst Type and Reaction Parameters on One-Step Acrylation of Soybean Oil. *ACS Sustain. Chem. Eng.* **2014**, *2*, 181–187.
57. Zou, K.; Soucek, M.D. UV-Curable Cycloaliphatic Epoxide Based on Modified Linseed Oil: Synthesis, Characterization and Kinetics. *Macromol. Chem. Phys. Homepage* **2005**, *206*, 967–975.
58. Kalita, D.; Tarnavchyk, I.; Webster, D.C.; Chisholm, B.J. Synthesis and evaluation of novel plant oil-based polymers as binders for artist paints: Controllable drying behavior and low yellowness. *Prog. Org. Coat.* **2022**, *163*, 106607.
59. Kalita, D.J.; Tarnavchyk, I.; Sibi, M.; Moser, B.R.; Webster, D.C.; Chisholm, B.J. Biobased poly(vinyl ether)s derived from soybean oil, linseed oil, and camelina oil: Synthesis, characterization, and properties of crosslinked networks and surface coatings. *Prog. Org. Coat.* **2018**, *125*, 453–462.
60. Thomas, J.; Patil, R. Enabling Green Manufacture of Polymer Products via Vegetable Oil Epoxides. *Ind. Eng. Chem. Res.* **2023**, *62*, 1725–1735. [[CrossRef](#)]
61. Dinu, R.; Briand, N.; Mija, A. Influence of Keratin on Epoxidized Linseed Oil Curing and Thermoset Performances. *ACS Sustain. Chem. Eng.* **2021**, *9*, 15641–15652. [[CrossRef](#)]
62. Mauro, C.D.; Malburet, S.; Graillot, A.; Mija, A. Recyclable, Repairable, and Reshapable (3R) Thermoset Materials with Shape Memory Properties from Bio-Based Epoxidized Vegetable Oils. *ACS Appl. Bio Mater.* **2020**, *3*, 8094–8104. [[CrossRef](#)]
63. Mauro, C.D.; Malburet, S.; Genua, A.; Graillot, A.; Mija, A. Sustainable Series of New Epoxidized Vegetable Oil-Based Thermosets with Chemical Recycling Properties. *Biomacromolecules* **2020**, *21*, 3923–3935. [[CrossRef](#)]
64. Thomas, J.; Nwosu, J.; Soucek, M.D. Acid-Cured Norbornylized Seed Oil Epoxides for Sustainable, Recyclable, and Reprocessable Thermosets and Composite Application. *ACS Appl. Polym. Mater.* **2023**, *5*, 2230–2242. [[CrossRef](#)]

65. Chen, Z.; Chisholm, B.J.; Patani, R.; Wu, J.F.; Fernando, S.; Jogodzinski, K.; Webster, D.C. Soy-based UV-curable thiol-ene coatings. *J. Coat. Technol. Res.* **2010**, *7*, 603–613.
66. Wu, Y.; Fei, M.; Chen, T.; Li, C.; Fu, T.; Qiu, R.; Liu, W. H-bonds and metal-ligand coordination-enabled manufacture of palm oil-based thermoplastic elastomers by photocuring 3D printing. *Addit. Manuf.* **2021**, *47*, 102268.
67. Dai, J.Y.; Liu, X.Q.; Ma, S.Q.; Wang, J.G.; Shen, X.B.; You, S.S.; Zhu, J. Soybean oil-based UV-curable coatings strengthened by crosslink agent derived from itaconic acid together with 2-hydroxyethyl methacrylate phosphate. *Prog. Org. Coat.* **2016**, *97*, 210–215.
68. Yang, X.F.; Cheng, F.; Fan, Y.X.; Song, Y.; He, N.; Lai, G.Q.; Gong, Z.S.; Shen, J.B. Highly transparent acrylate epoxidized soybean oil based UV-curable silicone-modified coatings with good thermal stability and flame retardancy. *Prog. Org. Coat.* **2022**, *165*, 106769.
69. Bas, türk, E.; Intan, T.; Güngör, A. Flame retardant UV-curable acrylated epoxidized soybean oil based organic-inorganic hybrid coating. *Prog. Org. Coat.* **2013**, *76*, 985–992.
70. Liu, H.J.; Liu, W.C.; Liu, S.J. Development of acrylated soybean oil-based UV-curable coatings with high impact strength from low viscosity oligomer. *J. Appl. Polym. Sci.* **2018**, *135*, 45698. [[CrossRef](#)]
71. Ge, X.Y.; Yu, L.; Liu, Z.S.; Liu, H.S.; Chen, Y.; Chen, L. Developing acrylated epoxidized soybean oil coating for improving moisture sensitivity and permeability of starch-based film. *Int. J. Biol. Macromol.* **2019**, *125*, 370–375. [[CrossRef](#)]
72. Wu, B.; Sulfi, A.; Biswas, R.G.; Hisatsune, A.; Paquette, V.M.; Ning, P.; Soong, R.; Dicks, A.P.; Simpson, A.J. Direct Conversion of McDonald's Waste Cooking Oil into a Biodegradable High-Resolution 3D-Printing Resin. *ACS Sustain. Chem. Eng.* **2020**, *8*, 1171–1177. [[CrossRef](#)]
73. *China Standard GB/T 1727-1992*; General Preparation of Paint Film. Ministry of Chemical Industry of the People Republic of China: Beijing, China, 1992.
74. *China Standard GB/T 5532-2008*; Animal and Vegetable Fats and Oils—Determination of Iodine Value. Ministry of Chemical Industry of the People Republic of China: Beijing, China, 2008.
75. *China Standard GB/T 1677-2008*; Determinating the Epoxy Value of Plasticizers. Ministry of Chemical Industry of the People Republic of China: Beijing, China, 2008.
76. *China Standard GB 5009.168-2016*; National Standards for Food Safety—Determination of Fatty Acids in Food. Ministry of Chemical Industry of the People Republic of China: Beijing, China, 2016.
77. *China Standard GB/T 14571.3-2008*; Ethylene Glycol for Industrial Use—Determination of Content of Total Aldehydes Present—Spectrophotometric Method. Ministry of Chemical Industry of the People Republic of China: Beijing, China, 2008.
78. *China Standard GB/T 1040.2-2006*; Plastics—Determination of Tensile Properties—Part 2: Test Conditions for Moulding and Extrusion Plastics. Ministry of Chemical Industry of the People Republic of China: Beijing, China, 2006.
79. *China Standard GB/T 6739-2006*; Paints and Varnishes—Determination of Film Hardness by Pencil Test. Ministry of Chemical Industry of the People Republic of China: Beijing, China, 2006.
80. *China Standard GB/T 9286-1998*; Paints and Varnishes—Cross Cut Test for Films. Ministry of Chemical Industry of the People Republic of China: Beijing, China, 1998.
81. *China Standard GB/T 1732-2020*; Determination of Impact Resistance of Film. Ministry of Chemical Industry of the People Republic of China: Beijing, China, 2020.
82. *China Standard GB/T 5209-1985*; Paints and Varnishes—Determination of Resistance to Water—Water Immersion Method. Ministry of Chemical Industry of the People Republic of China: Beijing, China, 1985.
83. *China Standard GB/T 1763-1979*; Methods of Test for Chemical Resistance of Paint Films. Ministry of Chemical Industry of the People Republic of China: Beijing, China, 1979.
84. *China Standard GB/T 9754-2007*; Paints and Varnishes—Determination of Specular Gloss of Non-Metallic Paint Films at 20, 60 and 85. Ministry of Chemical Industry of the People Republic of China: Beijing, China, 2007.
85. *China Standard GB/T 23983-2009*; Test Method for Yellowing Resistance of Wood Coatings. Ministry of Chemical Industry of the People Republic of China: Beijing, China, 2009.
86. Ha, Z.M.; Lei, L.; Zhou, M.Y.; Xia, Y.Z.; Chen, X.N.; Mao, P.; Fan, B.F.; Shi, S.X. Bio-Based Waterborne Polyurethane Coatings with High Transparency, Antismudge and Anticorrosive Properties. *ACS Appl. Mater. Interfaces* **2023**, *15*, 7427–7441. [[CrossRef](#)]
87. Zhou, M.Y.; Ha, Z.M.; Lei, L.; Xia, Y.Z.; Mao, P.; Chen, X.N.; Fan, B.F.; Shi, S.X. Castor oil-based transparent and omniphobic polyurethane coatings with high hardness, anti-smudge and anti-corrosive properties. *Prog. Org. Coat.* **2022**, *172*, 107120. [[CrossRef](#)]
88. Rabnawaz, M.; Liu, G.J.; Hu, H. Fluorine-Free Anti-Smudge Polyurethane Coatings. *Angew. Chem. Int. Ed.* **2015**, *54*, 12722–12727. [[CrossRef](#)] [[PubMed](#)]
89. Luo, H.H.; Wei, H.; Wang, L.; Gao, Q.; Chen, Y.; Xiang, J.; Fan, H.J. Anti-smudge and self-cleaning characteristics of waterborne polyurethane coating and its construction. *J. Colloid Interface Sci.* **2022**, *628*, 1070–1081. [[CrossRef](#)] [[PubMed](#)]
90. Hu, Y.; Liu, C.G.; Shang, Q.Q.; Zhou, Y.H. Synthesis and characterization of novel renewable castor oil-based UV-curable polyfunctional polyurethane acrylate. *J. Coat. Technol. Res.* **2018**, *15*, 77–85. [[CrossRef](#)]
91. Zhou, Y.M.; Feng, L.X.; Qu, J.Q. Preparation of high-performance epoxy soybean oil-based UV-curable oligomers and coatings. *J. Coat. Technol. Res.* **2023**, 1–11. [[CrossRef](#)]

92. Tang, J.J.; Zhang, J.S.; Lu, J.Y.; Huang, J.; Zhang, F.; Hu, Y.; Liu, C.G.; An, R.R.; Miao, H.C.; Chen, Y.Y.; et al. Preparation and Properties of Plant-Oil-Based Epoxy Acrylate-Like Resins for UV-Curable Coatings. *Polymers* **2020**, *16*, 2165. [[CrossRef](#)]
93. Liu, C.G.; Wang, C.; Hua, Y.; Zhang, F.; Shang, Q.Q.; Lei, W.; Zhou, Y.H.; Cai, Z.C. Castor oil-based polyfunctional acrylate monomers: Synthesis and utilization in UV-curable materials. *Prog. Org. Coat.* **2018**, *121*, 236–246. [[CrossRef](#)]
94. Cao, Z.Y.; Gao, F.; Zhao, J.Z.; Wei, X.; Cheng, Q.; Zhong, J.; Lin, C.; Shu, J.B.; Fu, C.Q.; Shen, L. Bio-Based Coating Materials Derived from Acetoacetylated Soybean Oil and Aromatic Dicarboxaldehydes. *Polymers* **2019**, *11*, 1089. [[CrossRef](#)]
95. Noè, C.; Lannucci, L.; Malburet, S.; Graillot, A.; Sangermano, M.; Grassini, S. New UV-Curable Anticorrosion Coatings from Vegetable Oils. *Macromol Mater. Eng.* **2021**, *306*, 2100029. [[CrossRef](#)]
96. Wu, Q.; Tang, J.J.; Zhang, J.; Wang, C.N.; Shang, Q.Q.; Feng, G.D.; Liu, C.G.; Zhou, Y.H.; Lei, W. High-Performance Soybean-Oil-Based Epoxy Acrylate Resins: “Green” Synthesis and Application in UV-Curable Coatings. *ACS Sustain. Chem. Eng.* **2018**, *6*, 8340–8349. [[CrossRef](#)]
97. Thames, S.F.; Yu, H. Cationic UV-cured coatings of epoxide-containing vegetable oils. *Surf. Coat. Technol.* **1999**, *115*, 208–214. [[CrossRef](#)]
98. Su, Y.; Ma, S.; Wang, B.; Xu, X.; Feng, H.; Hu, K.; Zhang, W.; Zhou, S.; Weng, G.; Zhu, J. High-performance castor oil-based polyurethane thermosets: Facile synthesis and properties. *React. Funct. Polym.* **2023**, *183*, 105496. [[CrossRef](#)]
99. Li, J.; Shen, H.; Zhao, Z.; Cao, D.; Zeng, M.; Cai, H.; Wei, J.; Fan, Q.; Deng, J.; Ming, F.; et al. Protective effects of Clostridium butyricum against oxidative stress induced by food processing and lipid-derived aldehydes in Caco-2 cells. *Appl. Microbiol. Biotechnol.* **2020**, *104*, 9343–9361. [[CrossRef](#)] [[PubMed](#)]
100. Zhao, D.; Le, T.; Larsen, L.B.; Li, L.; Qin, D.; Su, G.; Li, B. Effect of glycation derived from α -dicarbonyl compounds on the in vitro digestibility of β -casein and β -lactoglobulin: A model study with glyoxal, methylglyoxal and butanedione. *Food Res. Int.* **2017**, *102*, 313–322. [[CrossRef](#)]
101. Lynch, J.; Jin, L.; Richardson, A.; Conklin, D. Tobacco Smoke and Endothelial Dysfunction: Role of Aldehydes? *Curr. Hypertens. Rep.* **2020**, *22*, 73. [[CrossRef](#)]
102. Suh, K.S.; Choi, E.M.; Rhee, S.Y.; Kim, Y.S. Methylglyoxal induces oxidative stress and mitochondrial dysfunction in osteoblastic MC3T3-E1 cells. *Free Radic. Res.* **2014**, *48*, 206–217. [[CrossRef](#)]
103. Sena, C.M.; Matafome, P.; Crisóstomo, J.; Rodrigues, L.; Fernandes, R.; Pereira, P.; Seíça, R.M. Methylglyoxal promotes oxidative stress and endothelial dysfunction. *Pharmacol. Res.* **2012**, *65*, 497–506. [[CrossRef](#)]

Disclaimer/Publisher’s Note: The statements, opinions and data contained in all publications are solely those of the individual author(s) and contributor(s) and not of MDPI and/or the editor(s). MDPI and/or the editor(s) disclaim responsibility for any injury to people or property resulting from any ideas, methods, instructions or products referred to in the content.